CEPPAD

Comprehensive Energetic Particle and Pitch Angle Distribution Experiment on POLAR

J. B. BLAKE, J. F. FENNELL, L. M. FRIESEN, B. M. JOHNSON, W. A. KOLASINSKI, D. J. MABRY, J. V. OSBORN, S. H. PENZIN, E. R. SCHNAUSS and H. E. SPENCE
The Aerospace Corporation, Los Angeles, CA 90009, U.S.A.

D. N. BAKER
Goddard Space Flight Center, Greenbelt, MA 20771, U.S.A.

R. BELIAN, T. A. FRITZ, W. FORD, B. LAUBSCHER and R. STIGLICH
Los Alamos National Laboratory, Los Alamos, NM 87545, U.S.A.

R. A. BARAZE, M. F. HILSENRATH, W. L. IMHOF, J. R. KILNER, J. MOBILIA and D. H. VOSS
Lockheed Palo Alto Research Laboratory, Palo Alto, CA 94304, U.S.A.

A. KORTH, M. GÜLL and K. FISHER
Max-Planck-Institut für Aeronomie, Katlenburg-Lindau, Germany

and

M. GRANDE and D. HALL
Rutherford Appleton Laboratory, Chilton, Didcot, Oxon, U.K.

(Received 17 December, 1993)

Abstract. The CEPPAD Experiment consists of four sensors for investigating energetic particle phenomena on the POLAR mission. These sensors provide 3-D proton and electron angular distributions in the energy range of 20 keV to 1 MeV, energetic proton and electron measurements extending to energies greater than 10 MeV, high angular and time resolution measurements in the loss-cone, and data on energetic neutral particles. All sensors operate in conjunction with special on-board data processing units which control sensor data acquisition modes while performing in-flight data processing, data compression, and telemetry formatting. Presented here is a CEPPAD system overview together with descriptions of the individual sensors, the in-flight data processing, and examples of sensor calibration data.

1. Introduction

Some of the most challenging problems posed by the GGS program relate to dynamical processes that affect the entire magnetosphere. These include the overall response of the magnetosphere to changes in solar wind conditions, the complex reactions which occur during substorms, and the linkage between the outer parts of geospace and Earth's ionosphere. One of the themes of the GGS Mission is to make detailed *in situ* measurements of plasma, fields, and waves at multiple positions in the magnetosphere, and to correlate such observations. Energetic particles –

Space Science Reviews **71:** 531–562, 1995.

because of their unique properties – can be used as probes of the global state of the magnetosphere and thus provide a means of linking the *in situ* observations into a unified, comprehensive picture. As they are injected, accelerated, transported, and precipitated, these particles not only couple different elements of geospace, but also by virtue of the spatial scale of their adiabatic motion, serve as probes of regions remote from the spacecraft at which they are measured. In fact the study of energization processes is itself a fundamental goal of the GGS Program. The CEPPAD sensors are designed to provide continuous high resolution coverage of phase space (energy, pitch angle, and location) for both energetic ions and electrons. Such coverage is designed to make possible the unequivocal identification of access, acceleration, transport, and loss mechanisms for energetic charged particles in the magnetosphere. Since energetic particles precipitate deeply into Earth's atmosphere, they provide a means whereby processes in Geospace produce effects in Man's environment. Table I is a brief listing of science issues to be addressed by the CEPPAD investigation.

The CEPPAD investigation is an international collaboration between The Aerospace Corporation, Los Alamos National Laboratory (LANL), the Rutherford Appleton Laboratory (RAL), the Lockheed Palo Alto Research Laboratory (LPARL), the Max-Planck-Institut für Aeronomie (MPAe), the Goddard Space Flight Center (GSFC), and Boston University (BU). The CEPPAD body-mounted hardware consists of: the Imaging Proton Sensor (IPS), developed jointly by Aerospace and LPARL; the Imaging Electron Sensor (IES), developed jointly by LANL and RAL; the High Sensitivity Telescope (HIST), built by LANL; the Data Processing Unit (DPU), built by Aerospace with a power supply provided by the MPAe. The Source/Loss-Cone Energetic Particle Spectrometer (SEPS) mounted on the despun platform is provided primarily by LPARL with the data processor being provided by Aerospace.

2. System Overview

The CEPPAD Experiment is designed for the fast analysis of energetic electrons and ions with a complete coverage of the unit sphere in phase space plus a detailed 'picture' of the atmospheric loss cone. These capabilities are required to meet the majority of the scientific objectives of CEPPAD summarized in Table I. Dedicated sensor systems are provided for: (1) 20 to 500 keV electrons (IES) and protons (IPS) covering the unit sphere with comparable angular resolution for both species, (2) the high energy electron and proton component (HIST, $E_e \geq 350$ keV and $E_p \geq 3.25$ MeV), and (3) the loss cone measurements (SEPS). The sensor parameters are summarized in Tables II, III, IV and VI. The IPS and IES provide variable resolution coverage of the unit sphere by using the satellite spin and multiple detector 'pixels'. The HIST sensor measures the high energy electrons and protons perpendicular to the satellite spin axis. The SEPS sensor is mounted on the scan platform and

TABLE I

Summary of the scientific objectives of CEPPAD

Magnetopause structure and dynamics
– Particle transport across the magnetopause
– Remote boundary sensing
– Energetic particle layers
Magnetosheath, bow shock, and upstream regions
– Shock-accelerated particles
– Source of sheath energetic particles
– Correlations with upstream waves
Substorms and tail dynamics
– Plasma sheet energetic particle boundaries
– Energetic particle acceleration
– Hot plasma flow
– Plasma sheet thinning/expansion
Sources and sinks of particles
– Possible ionospheric sources
– Field-aligned particle streaming
– Pitch-angle evolution
– Solar, and Jovian particle access
– Adiabatic convection, and energization
– Convection boundaries
Wave-particle studies
– Natural particle precipitation
– Effect of man-made signals
– Upper atmospheric effects of precipitation
– Detailed loss-cone measurements
Energetic particles as tracers
– Measure magnetospheric compression by solar wind
– Magnetospheric dilation by ring current
– Drift-shell splitting effects to predict substorms
– Global field line modeling
– Location of drift boundaries
– Remote sensing plasmapause, plasma sheet, magnetosphere
Radial transport
– Radial-diffusion coefficients
– Convection of tail-accelerated particle
– Test particle adiabaticity
– Map morphology of nightside acceleration
– Source of high energy ($E > 1$ MeV) particles
Relativistic electron effects
– Relativistic electron entry/acceleration
– Relativistic electron trapping, and diffusion
– Auroral zone electron precipitation spikes
– Ion-cyclotron wave interactions
– Relativistic electron coupling to middle atmosphere

images energetic electrons and protons with trajectories roughly parallel (and anti-parallel) to the local magnetic field direction. SEPS can also image the charge-exchanged ions from the ring current, under appropriate conditions.

The IES, IPS, and SEPS provide the high temporal and spatial resolution required to support wave-particle studies, define the positron of magnetospheric boundaries, and sample large volumes of the magnetosphere. Distant acceleration processes can be sensed by using the high velocity of energetic electrons to provide nearly instantaneous signatures of distant active acceleration regions. The remote sensing of magnetospheric boundaries and processes can be detected by using the large energy-dependent gyroradii of the ions to sense the boundaries when they are still many kilometers distant from the satellite. The ions and electrons can also be used to observe the results of particle energization and injection from great distances, by observing the dispersive drift signatures imposed on the particle distributions by different physical processes such as the ion drift echoes often generated by substorm processes. A detailed description of the individual sensors, including their sensitivity and temporal- spatial resolutions is given below.

The CEPPAD Experiment payload consists of three separate boxes, as shown in Figure 1. Two (IPS/DPU and IES/HIST) are mounted on the spacecraft body, and one (SEPS) on the despun platform of the POLAR satellite. Figure 2 is a photograph of the body-mounted sensors, with the IES/HIST shown at the top, and the IPS/DPU, shown bolted to its storage fixture, at the bottom. All power, commands, and telemetry are routed to and from the body-mounted sensors through a single DPU. The SEPS instrument, whose photograph appears in Figure 3, communicates with the spacecraft via its own DPU, and can also use some of the telemetry allocated to PIXIE (Polar Ionosphere X-ray Imaging Experiment) when the latter is not imaging due to a high radiation background.

3. Body-Mounted Sensor Complement

As mentioned above, the body-mounted sensor package is made up of the IPS, IES, and HIST, communicating with the spacecraft via a single DPU. A brief description of the individual sensors and the DPU is given below, followed by a discussion of data handling, telemetry, and command software.

3.1. Imaging proton sensor (IPS)

The IPS consists of the Sensor Head Assembly (SHA) with three identical sensor heads, the Signal Conditioning Unit (SCU), and the Ion Pulse Pre-Processor (IPP). The sensor heads lie directly behind the three distinctive sun-shade structures attached to the SHA, as seen at the lower right-hand portion of Figure 2. The IPS measures ion spectra over the energy range of 20–1500 keV, with almost 4π sr coverage within a single 6 s spin period. Table II is a summary of the IPS measurement parameters.

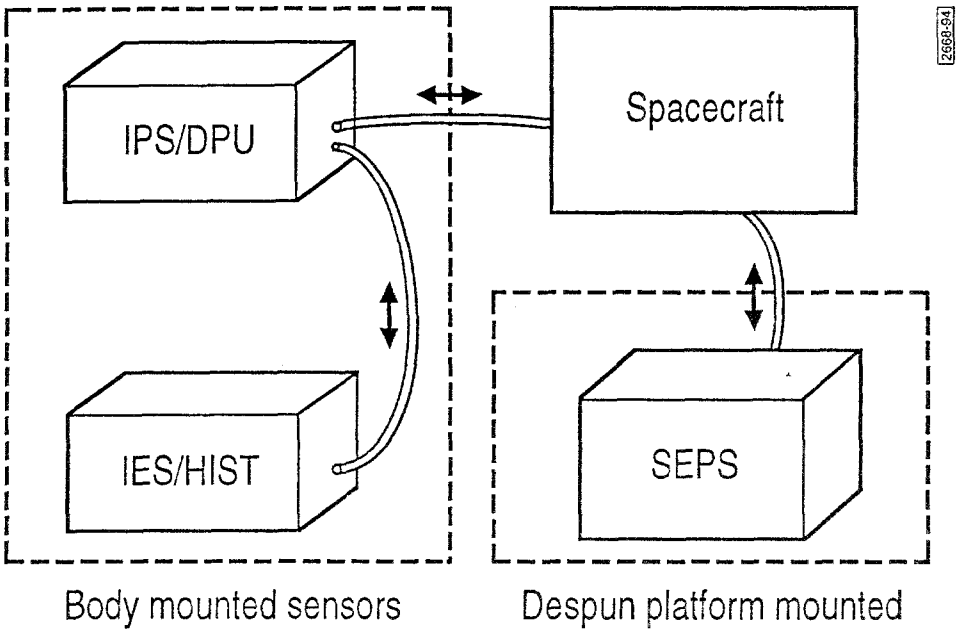

Fig. 1. A schematic view of the CEPPAD experiment.

TABLE II

IPS parameters

Particles detected	Protons
Energy range (keV)	20–1500
Energy resolution (keV, FWHM)	6
Number of energy channels (log/linear)	16
Field of view each large pixel (deg)	$12° \times 20°$
Complete field of view	$12 \times 180°$
Number of pitch angle channels	9×32 sectors
Duty cycle	100%
Large pixel geometric factor (cm^2 sr)	2.8×10^{-3}
Small pixel geometric factor (cm^2 sr)	2.8×10^{-4}
Number of large area pixels	9
Number of small area pixels	3
Number of background pixels	3

The sensor elements of the IPS are three custom designed, solid state detectors. A scale drawing of a single detector is shown in Figure 4. The detector, fabricated by Micron, Ltd., is a fully depleted, 150 mm thick, ion-implanted silicon-strip detector with six individual pixels surrounded by a guard-ring structure. During

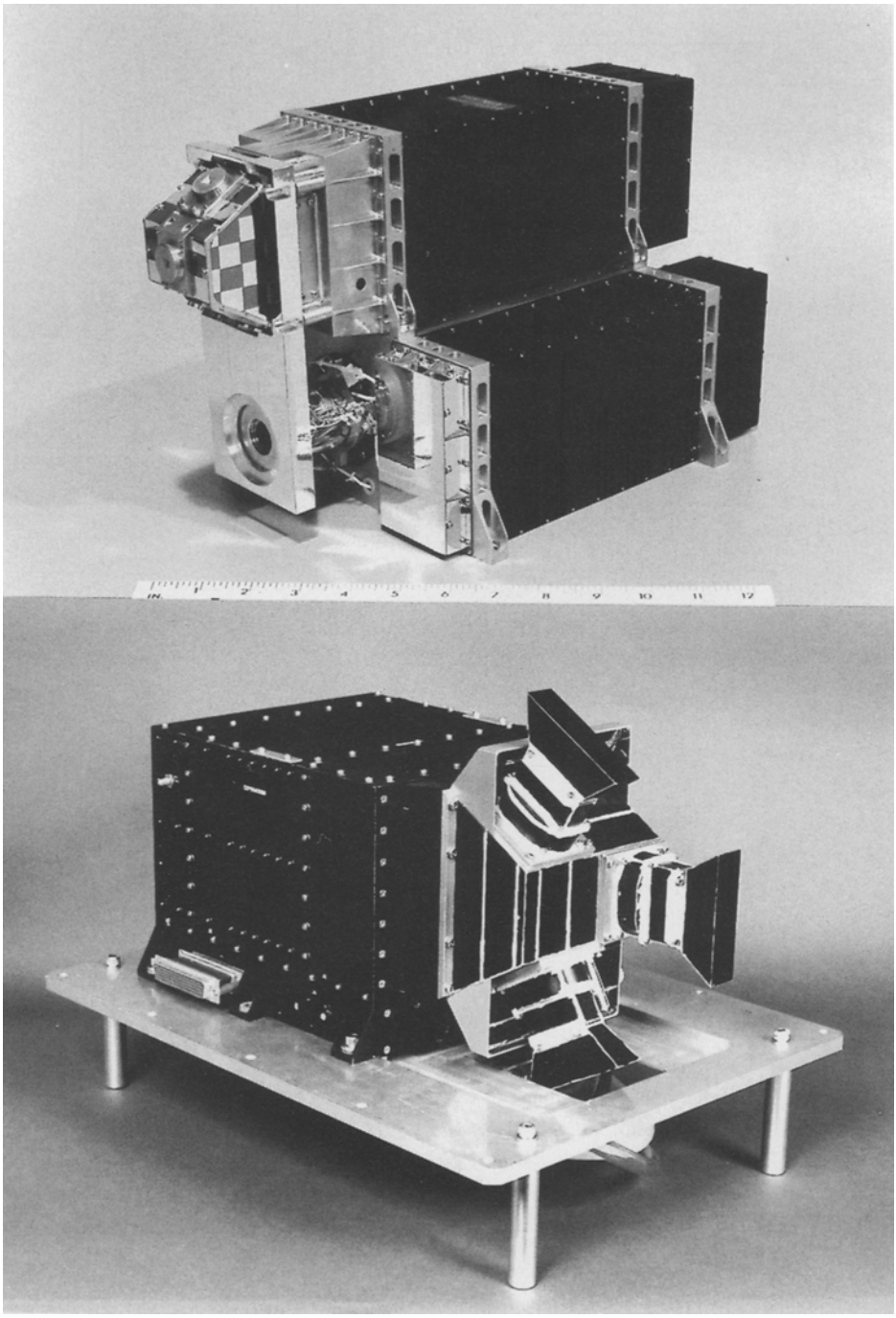

Fig. 2. Body-mounted CEPPAD sensors. *Top*: photograph of IES/HIST. *Bottom*: photograph of IPS/DPU in laboratory fixture.

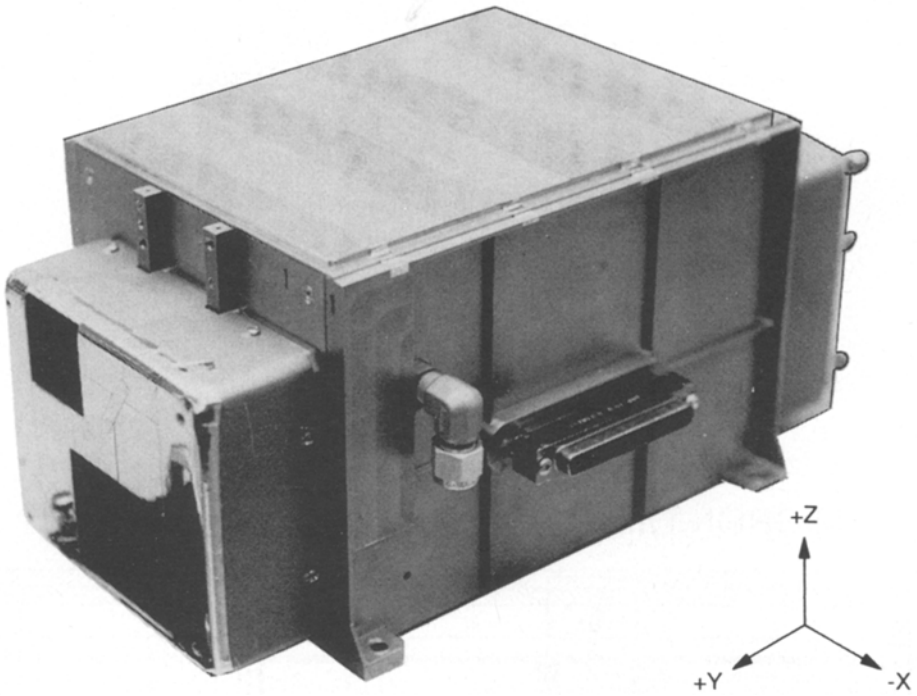

Fig. 3. Photograph of SEPS experiment.

TABLE III
IES parameters

Particles detected	Electrons
Energy range (keV)	20–400
Energy resolution (keV FWHM)	6
Maximum No. of energy bins (ADC)	256
Nominal No. of energy bins	15
Field of view each pixel (deg)	$30° \times 20°$
Number of pitch angle channels	9×32 sectors
Lifetime (2–100 ms integration)	2.4–55%
Large area geometric factor (cm^2 sr)	0.0017
Small area geometric factor (cm^2 sr)	0.00012
Number of small area pixels	9
Number of large area pixels	9
Angular coverage (1 spin period)	4π

design and fabrication, special effort was devoted to minimizing detector noise and the dead-layer thickness on the ion-implant side which faces the incident particle flux. Measurements performed with 30 keV protons on the flight detectors show

TABLE IV

HIST parameters

Particles detected	Electrons and protons
Electron energy range	350 keV–10 MeV
Proton energy range	3.25 MeV–80 MeV
Max. No. of energy bins (ADC) (electrons and protons)	256
Nominal No. of energy bins (log/lin; electrons and protons)	16
Field of view (deg)	26° conical
Number of pitch angle sectors	16
Geometric factor	0.088 cm^2 sr

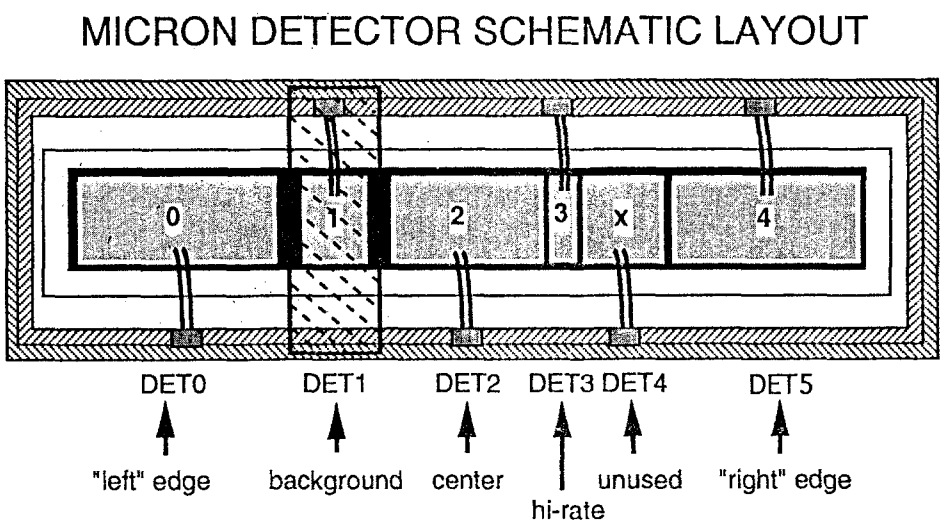

Fig. 4. Scale drawing of a single IPS detector showing the six pixels surrounded by the guard ring.

noise to be less than 5 keV (FWHM) at room temperature, and the dead-layer thickness approximately 5 keV. With these parameters, a proton-energy detection threshold of 20 keV can be readily achieved, even at room temperature. The large pixels marked 0, 2, and 4 in Figure 4 are sized to yield equal geometric factors for particles incident through the collimator assembly described below. A shielded background pixel (No. 1) monitors penetrating radiation, and a very small pixel (No. 3) can be used under conditions of high counting rate.

Figure 5 shows the mechanical assembly of a single head, with emphasis on the elements which define the detection geometry. Two stacks of blackened, brass anti-scattering baffles form the collimator assembly which defines the pixel fields of view and minimizes transmission of scattered sunlight. As depicted in Figure 5, a

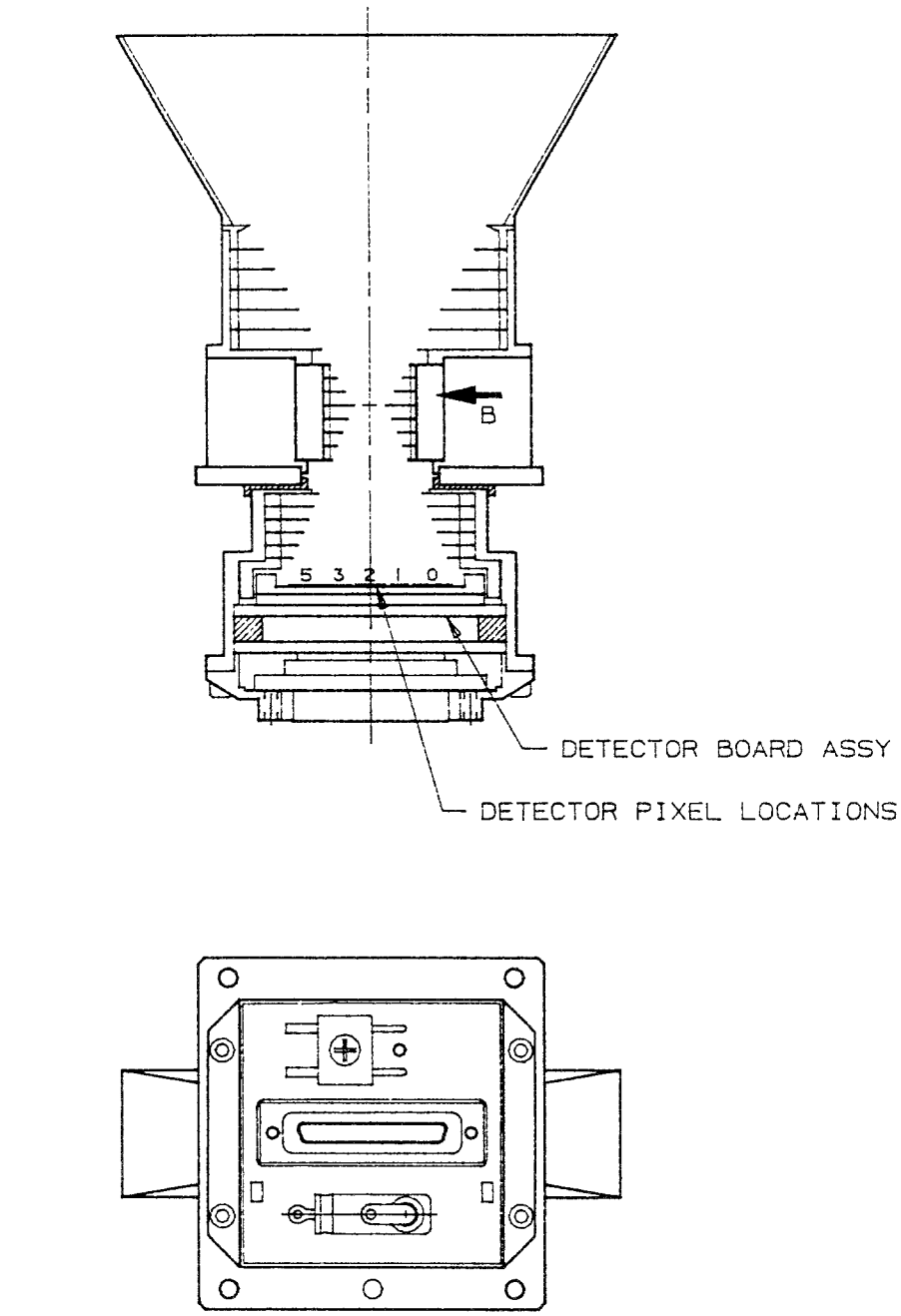

Fig. 5. Assembly drawing showing two views of a single IPS head.

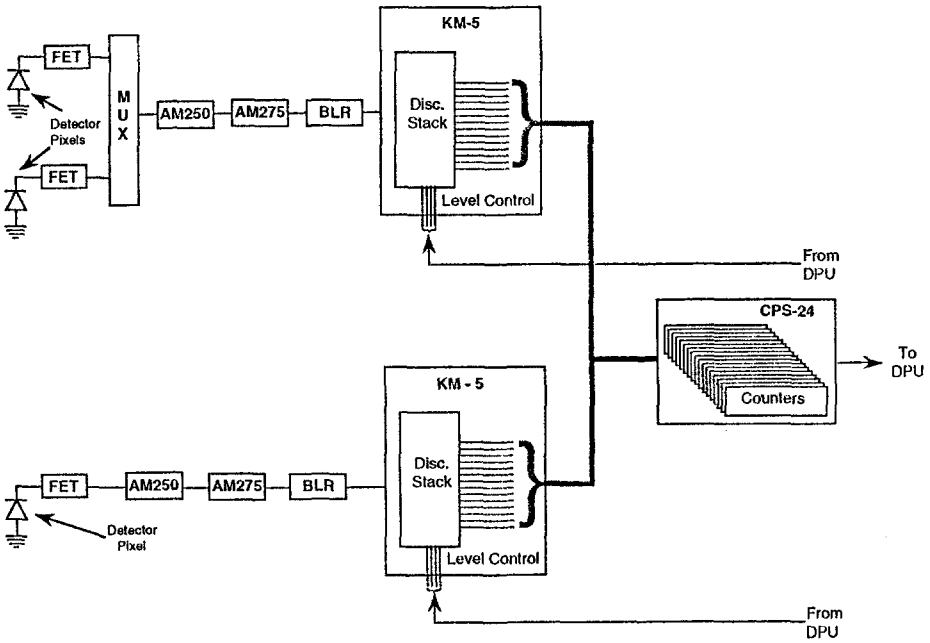

Fig. 6. Examples of MUXed and dedicated IPS detector channels in block-diagram form.

strong permanent magnet, with its pole-pieces placed at the center of the collimator assembly, is used to sweep out electrons with energies below approximately 1 MeV. To further reduce possible access of scattered sunlight while the Sun is outside the direct field of view, a shade with blackened and serrated inside surfaces is attached at the collimator entrance. Data obtained when the Sun is within the collimator field of view are discarded altogether. During direct sunlight exposure, the analog electronics are driven into saturation. The recovery time for each affected pixel is approximately 300 ms (or $\sim \frac{1}{20}$ of an anticipated 6-s spin period).

Two small printed-circuit boards are located inside the head assembly. One serves as the detector mount, containing also the coupling capacitors and the detector-biasing networks. The other board holds the calibration-signal routing network (see IPP description below), and five field-effect transistor (FET), charge-sensitive preamplifier stages which feed preamplifier and shaping amplifier chains located on three separate boards in the SCU. Figure 6 is a block diagram of two representative electronic chains, described later in some detail.

Four of the five FET outputs (corresponding to the one small and three large pixels) from each head are connected to three analog amplifier channels on a corresponding board in the SCU. One large and one small pixel in each head share a single amplifier channel via a two-fold multiplexer at the input to the AM250. The other two large pixels feed their own channels directly. There is a fourth channel on one of the three SCU boards, to which the background pixels are connected

via a three-way multiplexer. All multiplexing is performed by command from the DPU. Figure 6 shows two of the ten electronic channels, one connected to two multiplexed pixels. All channels contain a preamplifier (AM250), two AM275 shaping amplifiers (shown as one block in Figure 6), and a base-line restorer (BLR). These are commercially available items, manufactured by Amptek Inc. The SCU boards together with the two IPP boards form a single, removable stack in a separate compartment within the IPS/DPU box, directly behind the SHA.

Pulse height analysis of signals from the ten SCU channels occurs in the IPP. Each SCU channel is connected to a custom gate-array chip (KM-5) developed jointly with KMOS, Inc., as shown in Figure 6. A stack of discriminators is built into the chip, forming 16 adjacent energy bins. The energy (i.e., amplitude) threshold and range of the analyzer can be adjusted by sending digital commands to digital-to-analog converters (DACs) internal to the chip. It is also possible to select by command one of two resistor chains on the chip, providing linear (ΔE=constant) or logarithmic ($\Delta E/E$=constant) bin spacing. Output logic pulses from individual energy bins are accumulated in high rate, 24-bit scalers and read out from the latter by the DPU at time intervals controlled by command tables stored in the DPU memory. Nominally, that interval is 1/32 of the spin period. The IPP also serves as a calibration source for the IPS heads. Pulses with two fixed, precision amplitudes at 90 keV and 420 keV are available. A variable amplitude pulse generator, controlled by the DPU via an 8 bit DAC, also provides calibration signals on command.

Figure 7 shows measured angular responses of the IPS primary pixels (0, 2, and 4) as functions of the polar angle (actually its complement) with respect to the spin axis. These are responses to a highly collimated, parallel beam of 30 keV protons that uniformly fills the entrance aperture field of view (FOV). Each primary pixel has a 20-deg full-width-at-tenth-max triangular response. The pinhole optics defined by the entrance slit size, focal plane distance, and pixel location on the focal plane produce cleanly separated responses (crossing at the tenth-max level) between adjacent primary pixels. As a result, three non-overlapping 20-deg FOVs are obtained, yielding a 60-deg total polar FOV for each head. The three heads thus provide complete, non-overlapping 180-degree polar coverage with nine, 20-deg FOVs. Responses of the background pixel (No. 1) and the high-counting rate pixel (No. 3), neither of which is shown, are also quasi-triangular and fall in polar-angle ranges between the primary pixel responses. All azimuthal (in the spin plane) angular responses are also triangular, with a full-width-at-tenth-max of 12 deg.

Figure 8 shows the *total* electron transmission through the collimators and magnets as a function of incident energy. The actual background in each pixel, and to an even greater extent in each energy channel, is therefore much smaller, and is a function of channel number.

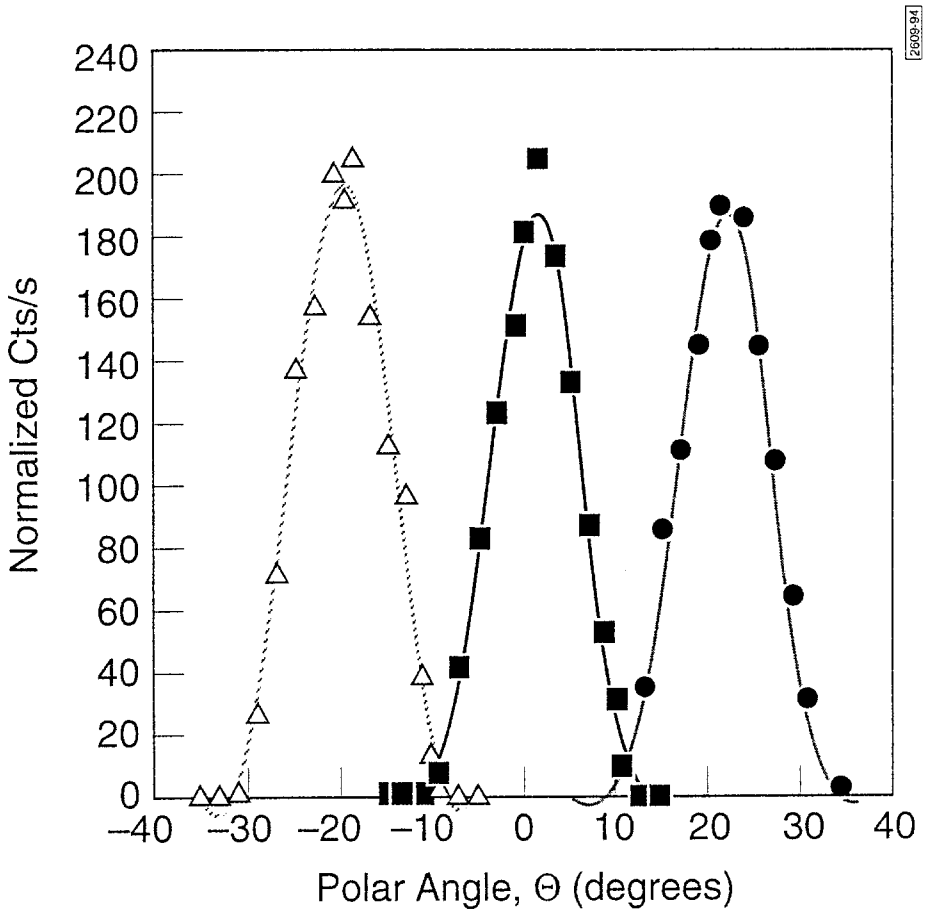

Fig. 7. Plot of the measured angular response of the IPS to 30 keV protons.

3.2. IMAGING ELECTRON SENSOR (IES)

The IES concept is very similar to that of the IPS. Ion-implanted, solid-state detectors, having a 0.5 cm×1.5 cm planar format with three individual elements, form an image plane behind an extremely narrow slit (pinslit). There are three such pinslit systems in the IES sensor head. Each system divides a 60° segment into three angular intervals. A schematic cross-section of an IES is shown in Figure 9. The three pinslit systems are arranged in the configuration depicted in Figure 10. Together, they provide electron measurements over a 180° polar $\times \sim 40°$ azimuthal field of view. Since the IES is mounted on the body of the rotating POLAR spacecraft, this field of view provides approximately 4π coverage during every spin period. The 500 μm ion-implanted silicon detectors (supplied by Canberra, Inc.) are covered with a 500 mg–cm^{-2} layer of aluminum. This thick contact, together with a 2200 nanometer aluminum-equivalent light shield,

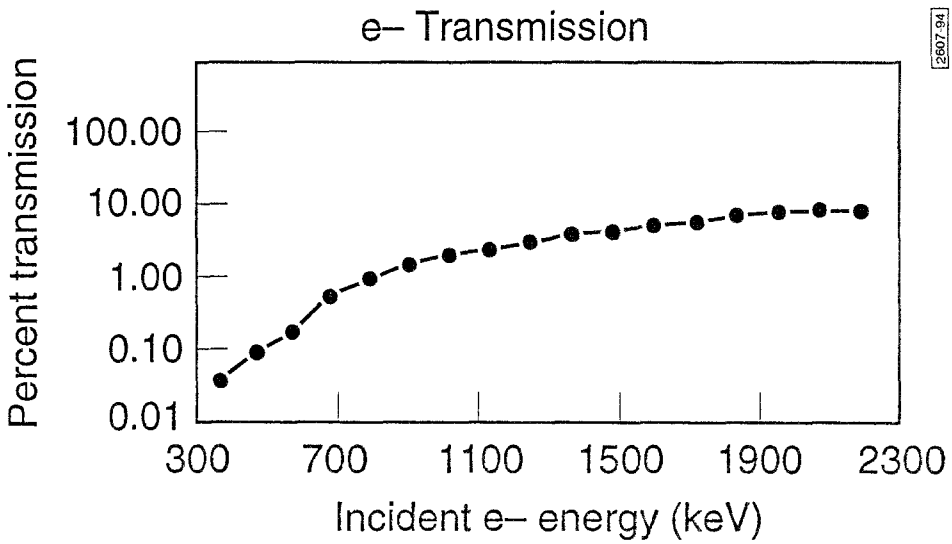

Fig. 8. Plot of the total transmission of electrons through an IPS collimator as a function of energy.

greatly reduces contamination from protons with energies above 375 keV. Without this shielding the trapped proton contribution to the instrument counting rate at L-values below 4.5 would be comparable to or greater than that from the electron flux.

The nine individual detectors in the three IES sensor heads are interrogated by a multi-channel, switched charge-to-voltage converter (SCVC) integrated circuit. For each detected particle the SCVC provides coded information on the pixel number and particle energy. This information is then digitized to 8-bits and transferred to the DPU for further processing. Figure 11 is a simplified block diagram of the principal elements of the IES electronic Signal Conditioning Unit (SCU). The initial amplifier stages for the nine detector channels and a multiplexer are implemented as an integrated circuit. This chip, a development of the Rutherford Appleton Laboratory, UK, is physically located in the sensor housing. The IES signal conditioning unit (SCU) performs two basic functions: first, it controls the digital sequencing of the SCVC chip, and second, it amplifies the output signals from the chip, digitizes them, and presents the digital data to the DPU.

Sixteen charge-sensitive preamplifier channels are available on the SCVC with a noise of 700 electrons rms (= 6 keV FWHM) at zero input capacitance. The total power consumed is about 10 mW. Only nine channels are actually used for the CEPPAD IES application. The essential functions of the SCVC chip are shown in the simplified circuit diagram presented in Figure 12. The charge generated in an active pixel of the solid-state detector by an incident particle is integrated and stored on the capacitor C2 following the preamp stage. This stored charge is compared with a background value stored on a companion capacitor Cl. The difference between these two values of charge is then strobed out and fed into a

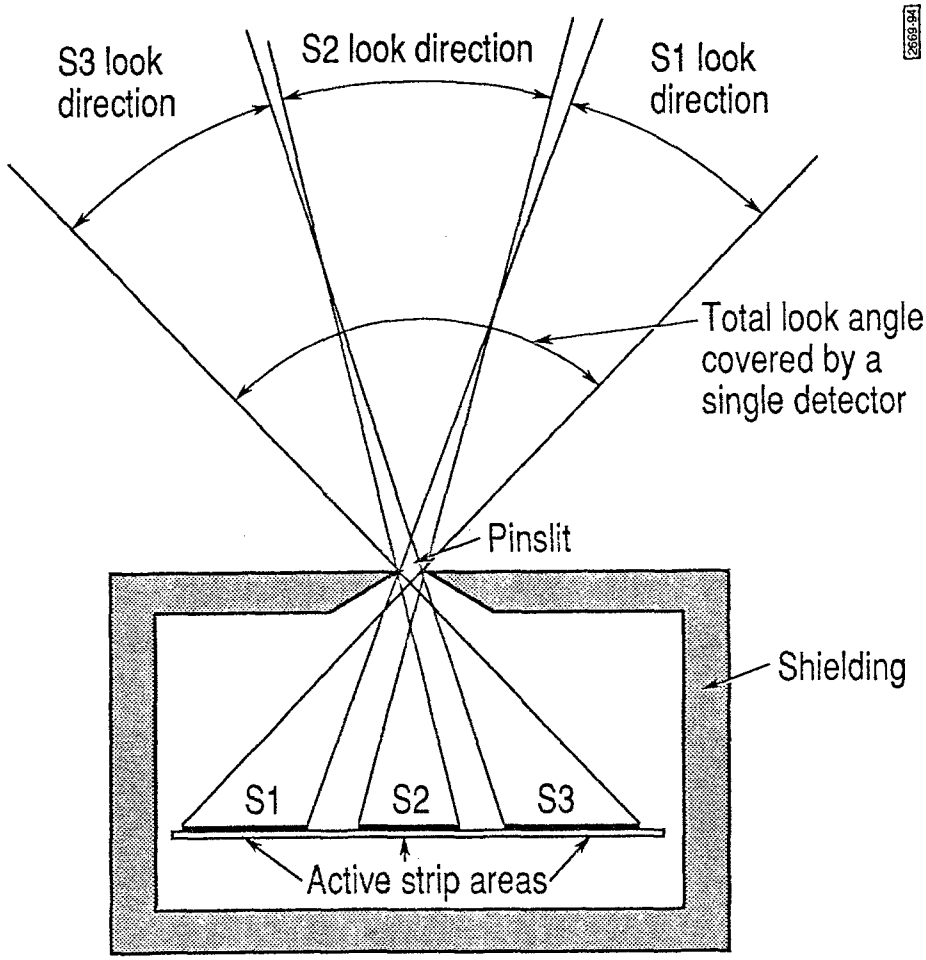

Fig. 9. Schematic drawing of the IES sensor configuration.

comparator circuit. From the comparator, the signal is read into an 8-bit analog-to-digital converter (ADC) giving the energy of the incident electron.

The charge generated by an incoming particle can be integrated by the SCVC for periods of 2, 10, 50, and 100 μs under DPU control. This capability is provided to minimize the effects of pileup and dead time. For example, in regions of high flux (e.g., trapped radiation belts) the lower integration times are used. As the spacecraft moves out of the high flux region, longer integration times might be used to reduce counting losses associated with the fixed readout time, thereby reducing the statistical errors in the acquired data. However, while increasing the system dead-time, the shorter time constant also tends to raise the system noise. It is the function of the DPU to optimize the integration time constant by monitoring the counting rates.

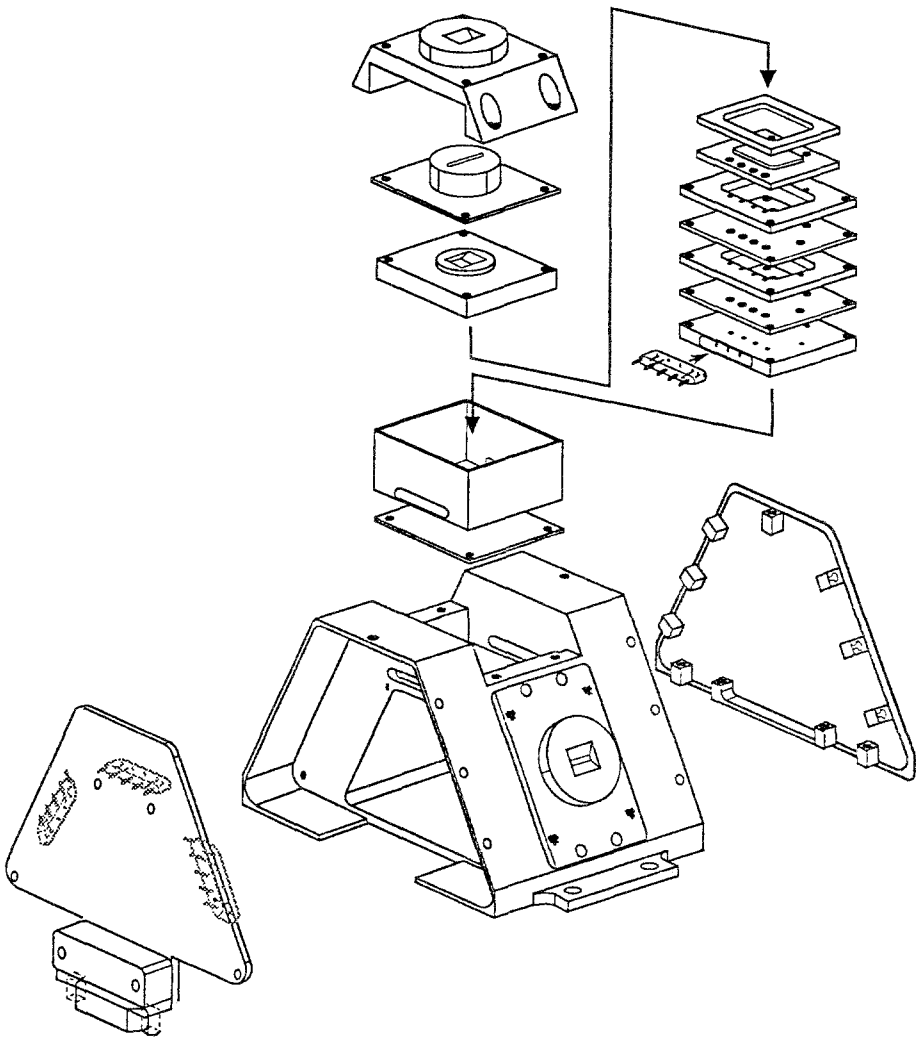

Fig. 10. Exploded view of an IES sensor head.

In the SCVC chip output there is an offset or pedestal value. This value is different for each channel, and depends somewhat on the integration time. The output of the IES SCU is a set of nine digital values corresponding to the sum of signal and pedestal values recorded since the previous readout. Each of the outputs, representing an energy measurement, is tagged with a four-bit direction (i.e. pixel) number to form an address pair combined into a 12-bit 'Direct Event' word in the Electron Pre-Processor (EPP) of the DPU. Since the pedestal values do not depend on time or temperature, they are subsequently subtracted out during the processing of the digitized signals by the EPP. The DPU can handle the IES data at a rate equal to or greater than 200 kHz, the maximum sampling rate of the SCVC.

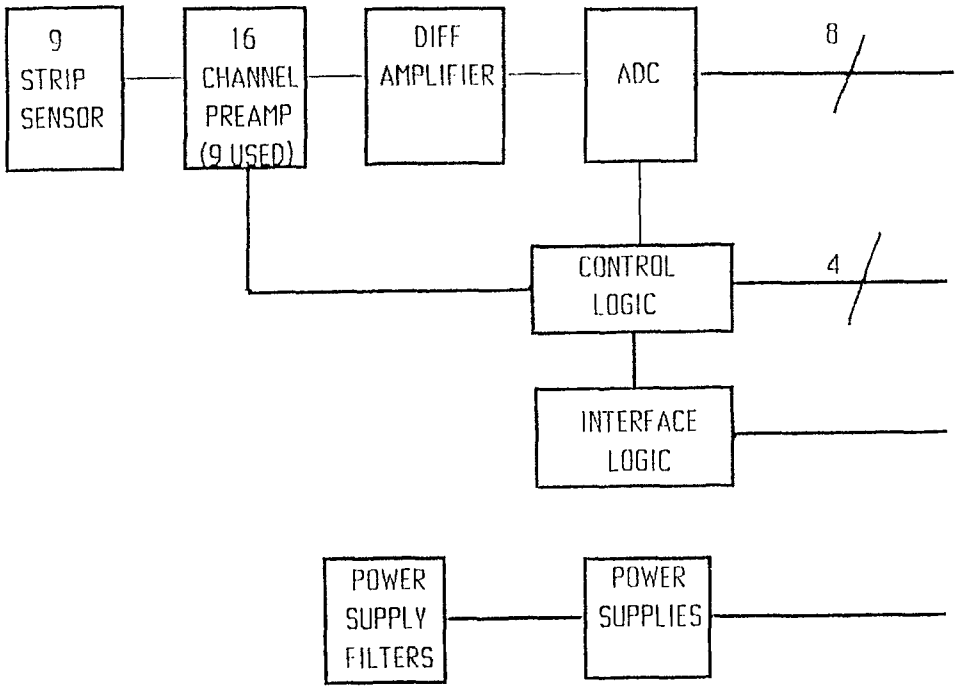

Fig. 11. Block diagram of IES electronics.

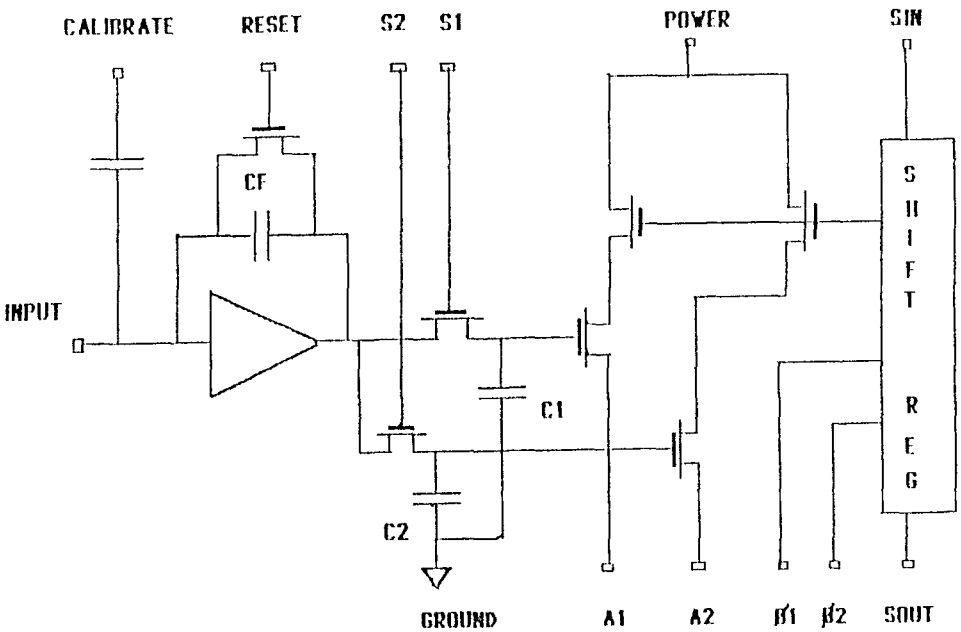

Fig. 12. A diagram of one of the sixteen identical channels on the RAL chip.

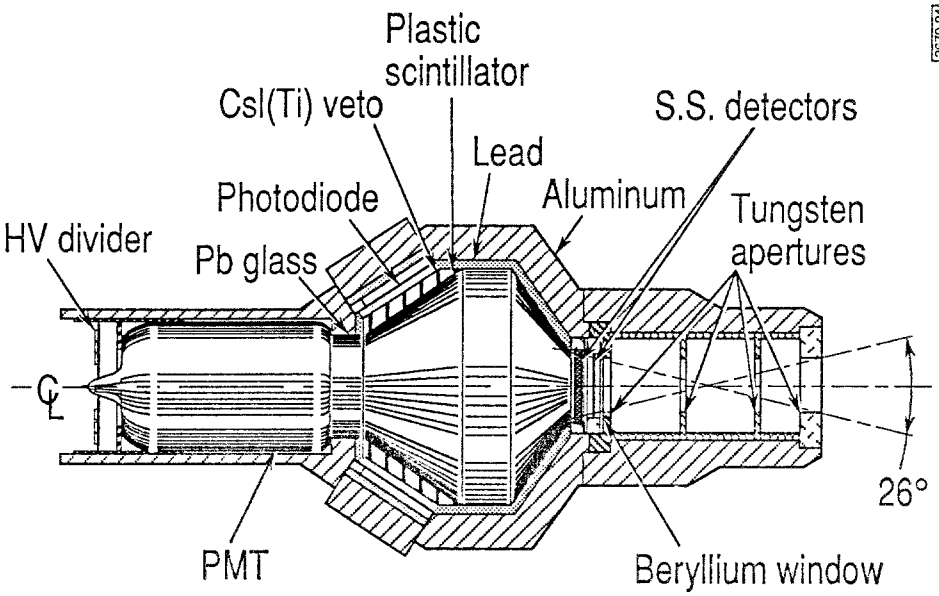

Fig. 13. A cross-section of the HIST sensor with the major components labeled.

Since the IES detector elements are very compact, it is not practical to test them with a pulser and charge terminators. Instead, during tests on the ground, the full system is stimulated with a set of radioactive sources which produce a series of gamma or x-ray lines in the 20 keV to a few hundred keV energy range. In this way it is possible to calibrate the IES system very accurately, demonstrate the linearity of the amplifiers, and measure the pedestal variation from channel to channel. In flight, a built-in calibration scheme similar to that of the IPS is used to correct for gain drifts in electronic system.

3.3. HIGH SENSITIVITY TELESCOPE (HIST)

Figure 13 is a schematic representation of the essential HIST elements The primary purpose of the HIST (High Sensitivity Telescope) is to accurately measure electrons from 350 keV to 10 MeV; protons from 3.25 to 80 MeV are also detected. The HIST contains three detector elements: a 300 μm thick, 300 mm^2 surface-barrier detector (Detector A); a 2000 μm thick 200 mm^2 surface barrier detector from ORTEC (Detector B), and a Bicron plastic scintillator viewed by a Hamamatsu R3668 photomultiplier tube (Detector C).

This design emerged from simulation runs with a Monte-Carlo particle code to estimate the instrument's response to electrons and protons in the energy range of interest. The results of these simulations are summarized in Figure 14, which shows the energy deposit by electrons and protons in each detector, as functions of the incident particle energy. A complex set of amplitude and coincidence-logic criteria for particle identification (ID tag) were derived from these results. These

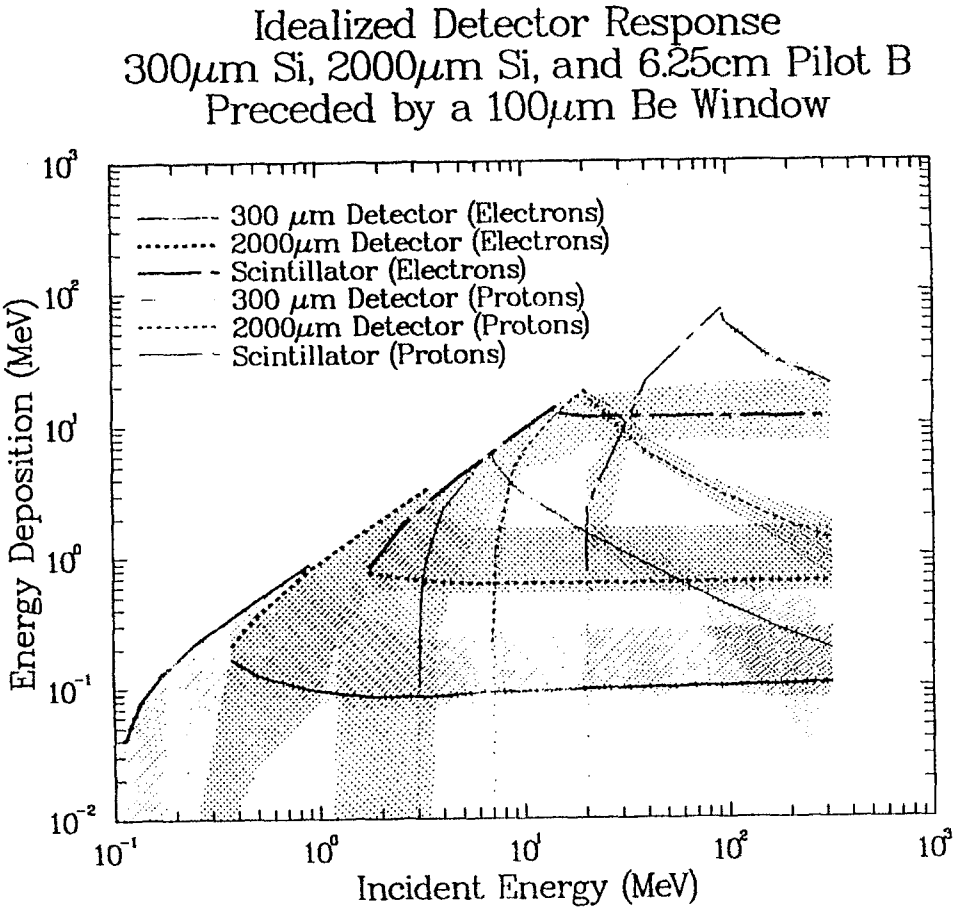

Fig. 14. Simulated response of the HIST to electrons and protons.

are summarized in Table V. The letters A, B, and C appearing in the logic criteria in Table V refer to detectors A, B, and C described above.

When a particle traverses one or more detectors (i.e., when an event occurs), the resulting analog signals from the three detectors are summed together, integrated, and digitized into 8 bits. These data are concatenated with the 4 bit ID tag representing the particle type and energy range. The resultant 12-bit word is transferred to the DPU on a parallel bus as a particle event. Pulses from several of the coincidence-logic circuits are accumulated in scalers and sent to the DPU at the boundary of each angular sector.

The HIST can be programmed to operate in up to 18 different modes via a 16 bit command word sent by the DPU. These modes provide great flexibility in the HIST operation. One example is a calibration mode in which the instrument looks only at the signals in the scintillator, where an internal ^{241}Am source provides a known signal input. This diagnostic allows correction for on orbit gain changes of the

TABLE V

HIST Energy Range Select Criteria

	4 BIT ID N2	N1	N0	TH	CRITERIA	8 BIT ENERGY	KEV/BIT
ELECTRON	0	0	0	0	$A_1 \cdot B_1 \cdot \overline{C_1} \cdot \overline{B_3} \cdot \overline{TH} \cdot \overline{D_1}$	350 keV - 2.5 MeV	10 keV/Bit
	0	0	1	0	$A_1 \cdot B_1 \cdot C_1 \cdot \overline{B_3} \cdot \overline{C_3} \cdot \overline{TH} \cdot \overline{D_1}$	350 keV - 2.5 MeV	10 keV/Bit
	0	1	0	0	$A_1 \cdot B_1 \cdot \overline{C_1} \cdot B_3 \cdot \overline{TH} \cdot \overline{D_1}$	1.2 MeV - 10 MeV	40 keV/Bit
	0	1	1	0	$(A_1 \cdot B_1 \cdot C_1 \cdot B_3) + (A_1 \cdot B_1 \cdot C_1 \cdot C_3) \cdot \overline{TH} \cdot \overline{D_1}$	1.2 MeV - 10 MeV	40 keV/Bit
ION	0	0	0	1	$A_1 \cdot \overline{B_1} \cdot \overline{C_1} \cdot TH \cdot \overline{D_1}$	1.0 MeV - 10 MeV	40 keV/Bit
	0	0	1	1	$A_1 \cdot B_1 \cdot \overline{C_1} \cdot TH \cdot \overline{B_4} \cdot \overline{D_1}$	1.0 MeV - 10 MeV	40 keV/Bit
	0	1	0	1	$A_1 \cdot B_1 \cdot \overline{C_1} \cdot TH \cdot B_4 \cdot \overline{D_1}$	8.0 MeV - 80 MeV	314 keV/Bit
	0	1	1	1	$A_1 \cdot B_1 \cdot C_1 \cdot TH \cdot \overline{D_1}$	8.0 MeV - 80 MeV	314 keV/Bit

$TH = A_H + B_H + C_H$

$A_1 = 90$ KeV

$B_1 = 160$ KeV

$C_1 = 160$ KeV

$B_3 = 1.10$ MeV

$B_4 = 5.56$ MeV

$C_3 = 1.10$ MeV

$A_H = 980$ KeV

$B_H = 3.62$ MeV

$C_H = 10$ MeV

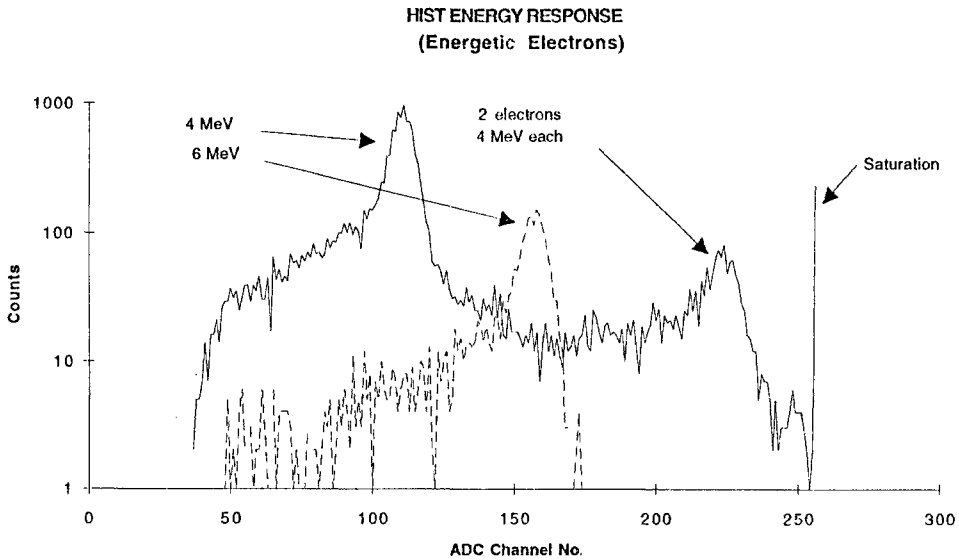

Fig. 15. Measured HIST response to 4 and 6 MeV electrons.

PMT by adjusting the PMT voltage (accomplished through other command-word bits). Other examples include modes for changing the discriminator levels and the possibility of disabling of the one or both solid-state detectors. The latter function is useful when the counting rates at low energy approach the limit where pileup and deadtime become a problem. Turning off the first detector (or both) prevents lower energy particles, which stop in the disabled detector(s), from being counted, thereby reducing the number (and rate) of events that the electronics must process. For diagnostic purposes, four 0–5 V analog housekeeping channel outputs are also generated by the HIST and digitized by the DPU.

The actual energy response of the sensor (originally calculated by the simulations) was measured in the course of extensive electron- and proton-beam calibrations using: the LANL and Aerospace beta-ray spectrometers (0.3–3.0 MeV electrons); the LANL Van de Graaff (3–20 MeV protons); the EG and G Linac (2.5–15 MeV electrons); and the LBL 88|| Cyclotron (16 to 50 MeV protons). Examples of the calibration results are shown in Figures 15 and 16. Figure 15 shows the energy response of the HIST to 4 and 6 MeV electrons. Figure 16 gives the angular response of the instrument for 1.6 MeV electrons with 3 types of ID tags.

3.4. DIGITAL PROCESSING UNIT (DPU)

The DPU is a rather sophisticated micro-computer which interfaces with the three CEPPAD sensors and the spacecraft power and telemetry buses. It performs on-board data processing, compression, formatting, and transfer to the spacecraft telemetry. In order to optimize these functions under changing conditions in

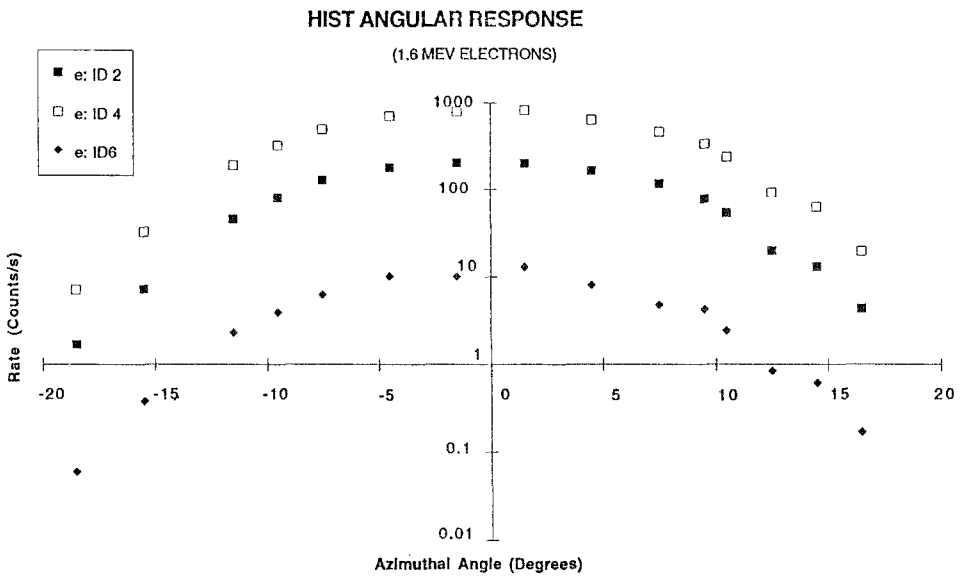

Fig. 16. Measured angular response of HIST to 1.6 MeV electrons.

orbit, the DPU accepts from the spacecraft new look-up table data and command sequences, for incorporation into software routines stored in DPU memory.

Physically, the system is made up of 8 boards: the CPU, Spacecraft Interface, IES Pre-Processor (EPP), HIST Pre-Processor (HPP), IPS Interface, Memory (2 boards), and the Power Supply. There are 512 Kbytes of Random Access Memory and 64 Kbytes of Pre-programmed Read Only Memory (PROM). Figure 16 is a functional block diagram of the DPU, summarizing the functions performed by the various DPU components. Since some acquaintance with the CPU, EPP, and HPP operation is needed for understanding the various sensor operating modes and data formats, brief descriptions of these units follow.

Located on the CPU board is a Harris HS80C86RH microprocessor with its support circuitry consisting of several field-programmable gate arrays and large scale integrated circuit components. The board is also equipped with a Clock Generator, 64 Kbytes of power-switched PROM, Direct Memory Access (DMA) hardware, 16 levels of interrupts, and six 16-bit counter-timers.

Initial boot programs and calibration tables for the DPU are located in the 64KB power switched PROM of the CPU board. After initial turn-on, the CPU downloads these initial data into the DPU RAM and turns off the PROM to save power. Program execution continues from RAM, where code and look-up table modifications can be performed on-orbit. A special keep-alive feature holds all

RAM contents intact during DPU turn-off, as long as a specially provided power line remains energized.

The CPU board also provides a 100 ms time base, a watch-dog timer, and a 16-level interrupt control system. The latter controls simultaneous background data transfer among all sensor and spacecraft interfaces with only occasional software support. If the software fails to reset the watch-dog timer during any given major frame, the timer forces a system reboot.

All communication with the IES sensor is handled by the EPP. One of several IES operating modes can be selected via serial command, including the choice of a large or small area pixel, calibration state, or charge integration time constant. A separate command echo interface allows for confirmation that the proper mode has indeed been implemented. In operation, the DPU changes the IES command mode on spin-period (6 s) boundaries, and echoes the current mode once per sector (187 ms). Statistics are maintained within the system software on the number of incorrect echoes.

A fast, parallel interface transfers particle data from the IES to the DPU. As described in Section 2.2, the SCVC interrogates the nine individual detector elements according to a sequential sampling scheme. For each detector, the Direct Event (DE) output to the DPU consists of detector number (4 bits) and energy (8 bits). Dedicated hardware, (including two 32 KByte banks of RAM) within the EPP allows for sustained data accumulation at rates higher than the 200 K samples s^{-1} output rate of the IES. The DE acquisition hardware is backed by a programmable look-up table which maps each event energy to one of 15 energy bins for each detector.

Each of the nine detectors (pixels) is assigned 15 distinct 24-bit RAM scalers corresponding to the 15 energy bins for each sector ($\frac{1}{32}$ of the spin period) within each of two RAM-scaler matrix banks. This translates to a total of 960 ($15 \times 32 \times 2$ scaler banks) scalers per detector. During each spin period, data are accumulated in one bank while being read out from the other. At the end of the period, the Sun pulse is used to toggle the two scaler banks.

The HPP board is very similar to the EPP, providing similar functions for the HIST sensor. For the HIST, the command echo also includes 16 countrate channels which correspond to the number of detected events meeting various coincidence criteria since the last readout. The count data are acquired once per sector ($\frac{1}{32}$ of spin period), incorporated in the telemetry stream as quarter-spin totals and used to automatically switch the HIST mode whenever the observed rates indicate the occurrence of excessive pulse pile-up.

As is the case for IES, the HIST parallel data interface generates 8 bits of amplitude information for each science data event, with 4 bits of tag ID. However, the information contained in the ID bits is different. One of the bits distinguishes between proton and electron events, while the other three indicate which logic equations were used within the sensor to determine the energy, i.e., gain and offset needed to convert amplitude value to energy in keV. For more information see

Table V and the discussion in Section 2.3. Like its IES counterpart, the HPP RAM scaler matrix consists of two banks toggled by the sun pulse between readout and acquisition modes. The primary function of the programmable look- up table for the HIST is to identify and bin all electron and proton events into two sets of 16 energy bins spanning the sensor energy range, by use of the gain and offset indicator bits of the tag ID. The counts corresponding to the 16 electron and 16 ion energy bins are accumulated in 32 24-bit scalers for each angular sector. For more information, see Section 2.3 and Table V.

3.5. COMMAND, TELEMETRY, AND DATA PROCESSING SOFTWARE

As described previously, the combined sensor payload has multiple look directions and energy bins for each of the three body-mounted sensors. The IPS sensor has 9 distinct look directions (and 3 background monitors), each of which give 16 differential energy bins. A separate IPS integral energy bin gives the integral countrate of the 14 highest energy bins for each look direction. The IES contains 9 distinct look directions, each giving 15 differential energy bins and an integral energy bin. The HIST sensor simultaneously produces 16 proton energy bins and 16 electron energy resolution bins. Therefore, the instantaneous data output from the combined payload is 346 values: 170 IPS values (17 energies x 10 look directions) plus 144 IES values (16 energies $\times$ 9 look directions) plus 32 HIST values (16 electrons and 16 protons).

The IPS and IES sensors provide a FOV of 180° relative to the spin axis of POLAR; therefore as POLAR spins with a 6-s period, a 4π image will be produced. On board, the DPU accumulates data in 24-bit counters. Each spin period can be subdivided by the DPU into 2^n equal angular intervals (sectors), where n can take on any integer value between 0 and 5. Thus, assuming the maximum number of 32 sectors per spin, the body-mounted CEPPAD payload would require $\sim$ 44.2 Kbits s^{-1} of telemetry to output 100% of the raw data. Unfortunately, only 3.2 Kbits s^{-1} are available. To reduce the raw data rate to fit within the available telemetry rate, three schemes are implemented within the software. First, all raw data items are quasi-logarithmically compressed from 24 to 8 bits before output. Second, individual energy bins can be assigned fewer than 32 sectors to further decrease the telemetry requirement, and third, data can be accumulated over multiple spins before it is output.

An illustrative example of how data acquisition, processing, and readout are accomplished, is provided by Table VI, which gives a concise description of the default, or normal science telemetry mode for the CEPPAD body-mounted sensors. Regardless of the telemetry mode, the available data will comprise IPS, IES, and HIST data. In the IPS section of Table VI, there are ten rows and seventeen columns which respectively correspond to the ten detector channels of the IPS, and seventeen energy bins of each channel (16 differential and 1 integral). The value of each element of this 10 $\times$ 17 matrix equals the even number of sectors assigned

TABLE VI

CEPPAD Normal Mode Telemetry

IPS (Imaging Proton Spectrometer)

IPS Detector Chan #	Channel ID	P0	P1	P2	P3	P4	P5	P6	P7	P8	P9	P10	P11	P12	P13	P14	P15	"P16" "integral"
	Eng Thresholds - Ep(keV)	20	25	31	38	47	58	72	90	111	138	171	212	263	326	403	500	
	# Spins/Data Sample	1	4	1	1	4	1	8	1	8	4	8	8	8	8	16	16	1
10	T1, C1, B1 Backgrounds	4	8	8	8	8	4	8	4	8	8	8	8	8	8	8	8	4
4	View Radially - Det# 4	16	16	32	16	16	16	16	16	16	16	16	16	16	16	16	16	32
3	3	16	16	32	16	16	16	16	16	16	16	16	16	16	16	16	16	32
5	5	16	16	32	16	16	16	16	16	16	16	16	16	16	16	16	16	32
6	6	16	16	16	16	16	16	16	16	16	16	16	16	16	16	16	16	32
7	7	16	16	16	16	16	16	16	16	16	16	8	8	8	8	8	8	32
0	View Along Spin - Det# 0	8	8	8	8	8	8	8	8	8	8	8	8	8	8	8	8	16
2	2	16	16	16	16	16	16	16	16	16	16	16	16	16	16	16	16	32
1	1	16	16	16	16	16	16	16	16	16	16	8	8	8	8	8	8	32
8	View Anti-Spin - Det# 8	8	8	8	8	8	8	8	8	8	8	8	8	8	8	8	8	16
	Bytes/spin (actual)	132	34	184	136	34	132	17	132	17	34	15	15	15	15	8	8	260

1188.0 bytes/spin

IES (Imaging Electron Spectrometer)

IES Large Det. Chan #	Channel ID	E0	E1	E2	E3	E4	E5	E6	E7	E8	E9	E10	E11	E12	E13	E14	"E15" "integral"
	Eng Thresholds - Ee(keV)	25	31	38	48	59	73	90	112	138	172	212	263	326	404	500	
	# Spins/Sample	1	1	8	1	8	1	8	1	8	4	8	8	8	16	16	1
1	View Anti-Spin - Det # 0	8	8	8	8	8	8	8	8	8	8	8	8	8	8	8	16
2	1	16	16	16	16	16	16	16	16	16	16	16	16	16	16	16	16
3	2	16	16	16	16	16	16	16	16	16	16	16	16	16	16	16	16
4	3	16	16	16	16	16	16	16	16	16	16	16	16	16	16	16	16
5	View Radially - Det # 4	16	16	16	16	16	16	16	16	16	16	16	16	16	16	16	16
6	5	16	16	16	16	16	16	16	16	16	16	16	16	16	16	16	16
7	6	16	16	16	16	16	16	16	16	16	16	16	16	16	16	16	16
8	7	16	16	16	16	16	16	16	16	16	16	16	16	16	16	16	16
9	View Along Spin - Det # 8	8	8	8	8	8	8	8	8	8	8	8	8	8	8	8	16
	Bytes/spin (actual)	128	128	16	128	16	128	16	128	16	32	16	16	16	8	8	144

944.0 bytes/spin

HIST (High Sensitivity Telescope)

Electrons

Channel ID	HP0	HP1	HP2	HP3	HP4	HP5	HP6	HP7	HP8	HP9	HP10	HP11	HP12	HP13	HP14	HP15	HP16
Eng Thresholds - Ee (MeV)	<1.0	3.00	3.74	4.65	5.79	7.21	8.97	11.17	13.91	17.32	21.56	26.85	33.43	41.62	51.82	64.51	80.32
# Spins/Sample	0	2	2	2	2	2	2	2	2	2	2	2	2	2	2	2	2
Angular Samples/Spin	1	16	16	16	16	16	16	16	16	16	16	16	16	16	16	16	16
Bytes/spin (actual)	0	8	8	8	8	8	8	8	8	8	8	8	8	8	8	8	8

128.0 bytes/spin

Protons

Channel ID	HE0	HE1	HE2	HE3	HE4	HE5	HE6	HE7	HE8	HE9	HE10	HE11	HE12	HE13	HE14	HE15	HE16
Eng Thresholds - Ep (MeV)	<.12	0.12	0.16	0.21	0.28	0.36	0.48	0.63	0.83	1.10	1.44	1.90	2.51	3.31	4.36	5.75	7.58
# Spins/Sample	0	2	2	2	2	2	2	2	2	2	2	2	2	2	2	2	2
Angular Samples/Spin	1	16	16	16	16	16	16	16	16	16	16	16	16	16	16	16	16
Bytes/data set	1	16	16	16	16	16	16	16	16	16	16	16	64	64	64	64	64

128.0 bytes/spin

Total Bit Rate: ~ 3183 bps

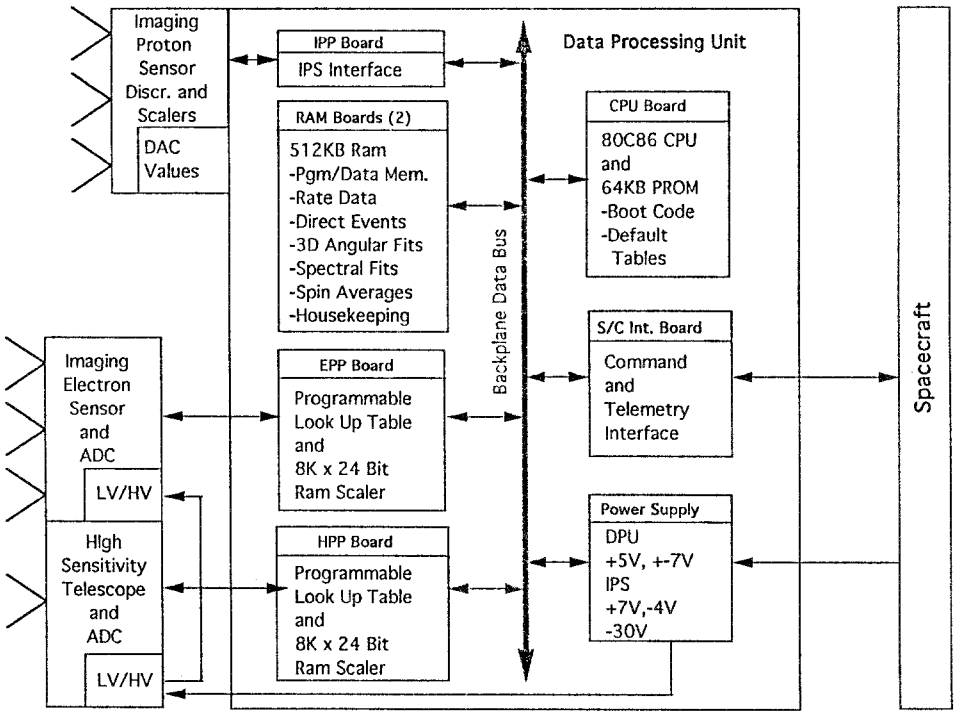

Fig. 17. A functional block diagram of the DPU.

to that detector-channel/energy-bin combination (or, the number of times that the corresponding 24-bit scaler is read out and cleared per spin period). At each sector readout time, data from the designated bins (as specified by the matrix elements of Table VI) are added to the appropriate sector locations in the DPU memory. Clearly, the values of the matrix elements control the angular resolution of data in the corresponding bins.

Temporal data resolution is controlled by values in the row labelled 'No. Spins/Data Sample' (first shaded row). Each number appearing in that row equals the number of spins over which all sector data for that energy bin, in all detector channels, are accumulated prior to transmission. For example, consider the matrix element corresponding to the intersection of the IPS detector-channel row 0, and energy-bin column P10. The element value is 8, meaning that for bin P10 of detector channel 0 there are 8 locations in memory, i.e. 8 sectors or angular samples, each 45 deg wide. The No. Spins/Data Sample is also 8 for column P10, indicating that counts in each of the 8 sectors or angular bins are summed over 8 spins (nominally 48 s), prior to transmission. Note that all angular bins for the P10 energy bins in all the detector channels have counts accumulated over 8 spins. A brief examination of the IES and HIST data processing matrices in Table VI shows that these data are handled in the same manner as the IPS data.

TABLE VII
SEPS parameters

	Electron telescope	Ion telescope
Energy range (MeV)	0.02–2.5	0.04–30
Energy resolution (keV)	1.0	15
Number of energy channels (log/linear)	32	32
Field of view (deg)	48° × 24°	20° × 20°
XY image matrix (pixels)	16 × 16	16 × 8
Detector area (cm^2)	12.5	6
Min. time sample period (ms)[a]	12.5	6
Geometric factor (cm^2 sr)[b]	0.02 to 0.0002	0.001
Total number of pixels	512	256

[a] Requires use of burst memory to output at this rate.
[b] Range based on use of aperture wheel.

Tables like Table VI are loaded into the DPU memory and are used by the microprocessor to control how the data are sectored, spin accumulated, and ordered within the telemetry stream. The shaded areas of the tables can be modified by ground command to produce different telemetry modes. The modified modes must meet the requirement that the total bytes allocated for IPS, IES, HIST electrons, and HIST protons not exceed 2389 bytes/spin. The CEPPAD DPU has 16 tables stored in PROM at launch, but each can be modified on orbit as needed.

4. Source/Loss-Cone Energetic Particle Spectrometer (SEPS)

4.1. INSTRUMENT DESCRIPTION

The SEPS instrument is located on the POLAR Despun Platform along with the auroral imagers, and is independent of the other CEPPAD sensors. SEPS measures both the energetic electron, and ion fluxes in the vicinity of the magnetic field-aligned loss, and source cone regions with high sensitivity, and with fine angular, and time resolution. The instrument parameters are given in Table VII. The basic view geometry of SEPS on the Despun Platform is illustrated in Figure 18 for a 9 R_e apogee polar orbit. The **A** vector indicates the aurora latitude direction, presumably the usual pointing direction of the Despun Platform while over the polar region, and **B** indicates the local magnetic field direction. The angle gamma is the offset angle between **A** and **B**. It is apparent that the **A** and **B** vectors are reasonably closely aligned over most of the orbit, and therefore within the SEPS field-of-view.

SEPS consists of two independent telescopes, one for electrons, and one for ions. A picture of the instrument is shown in the Figure 3. The electron telescope,shown

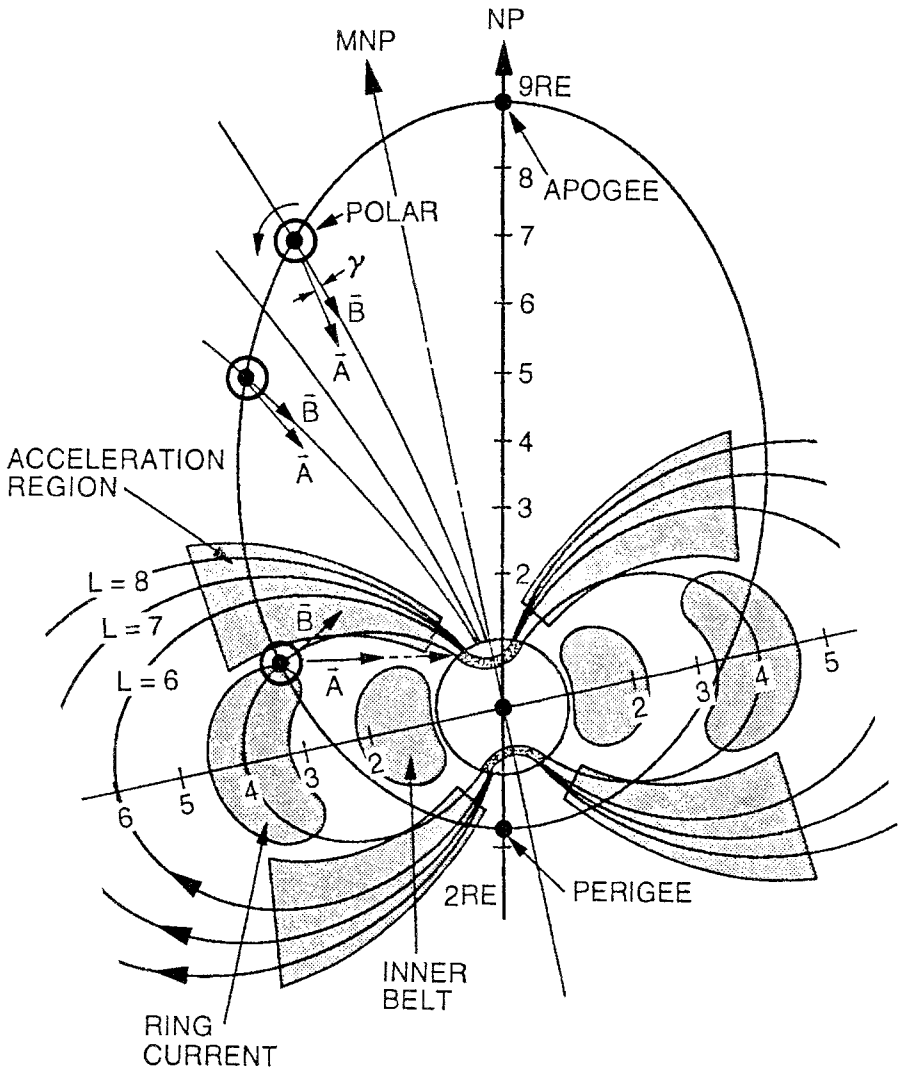

Fig. 18. View geometry of the SEPS, shown for time periods when POLAR is near apogee.

schematically in Figure 19, has twice the sensor area of the ion telescope, and uses aperture wheels to vary its dynamic range. Particle angular imaging is obtained using pinhole-camera apertures in front of XY position sensitive detectors marked T1–T4 in Figure 19. The ion telescope is similar to the electron telescope except for the reduced sensor area, and the fact that the aperture wheels are replaced by magnets which sweep out electrons. A unique feature of SEPSis the use of back

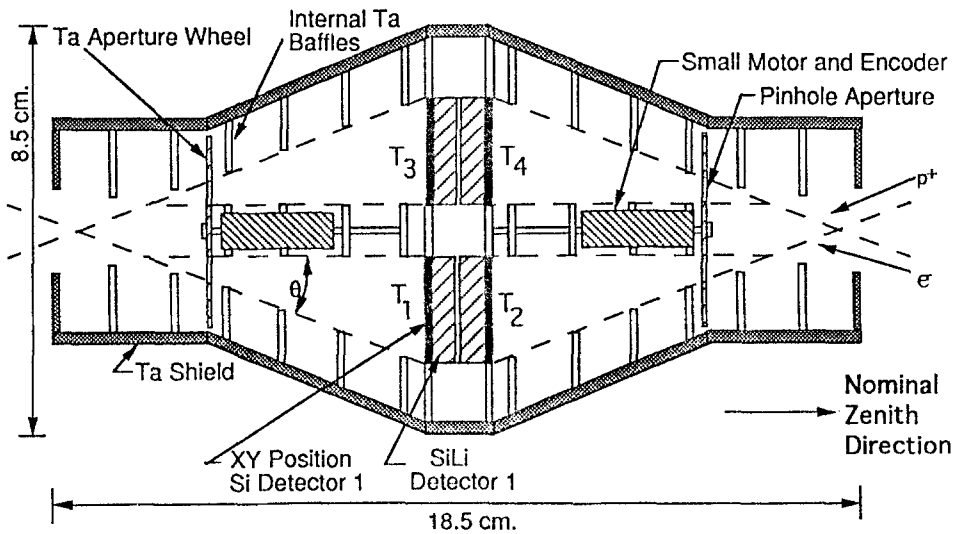

Fig. 19. Schematic view of SEPS electron telescope.

to back, dual collimators which permit entry of particles from opposite directions along the magnetic field into a common sensor telescope. The SEPS electron, and ion telescopes respectively have ±24 and ±10 deg fields of view in the orbit plane to cover a wide range of gamma angles. The respective ±12, and ±10 deg fields of view perpendicular to the orbit plane for the electron, and proton telescopes were chosen to cover the dipole wobble, and dynamic variations in the Earth's magnetic field. The coverage of the loss cone region is further increased when the Despun Platform is programmed for a fixed offset angle with respect to nadir at mid, and low latitudes. In the radiation belts, where the imaging photon instruments on the platform have limited yield because of the oblique auroral view and higher backgrounds, SEPS covers many interesting geospace environments.

SEPS is coaligned with the other three imagers on the platform, with the collimators looking along the $+Y$ (zenith), and $-Y$ (nadir) directions. A natural plane of symmetry exists about the $X - Z$ plane. To minimize shielding mass, the sensor telescopes are positioned in the center of the instrument with all of the electronic boards acting as secondary shields. The internal collimators and sensor telescopes are enclosed by tantalum shields to reduce background from penetrating particles and locally generated X-rays. To maximize the dynamic range and angular resolution, a variable aperture is included in both the zenith, and nadir directions of the electron telescope. The aperture size can be varied by two orders of magnitude using six pinhole sizes. Each aperture is driven by a 3 phase, No. 5 size stepper motor having 15 deg steps. An inline potentiometer is used to read the absolute angle. The ion telescope uses a strong broom magnet to sweep out electrons. Since the ion telescope is also sensitive to energetic neutrals, care must be taken to subtract the magnetic field aligned component from the remotely sensed ENA (energetic

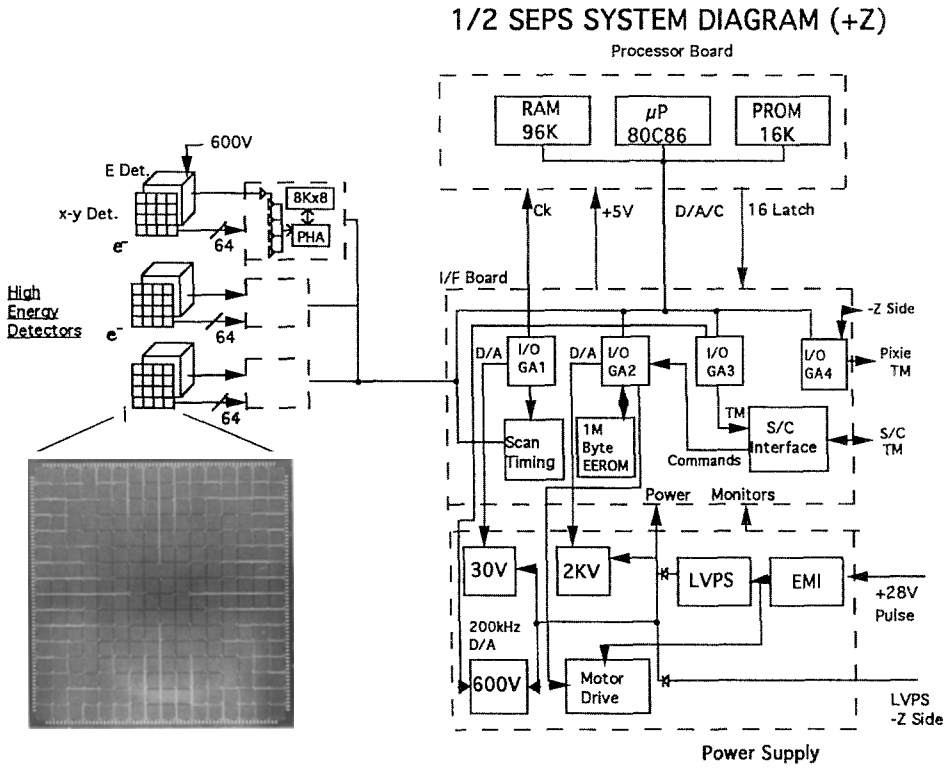

Fig. 20. Block diagram of $\frac{1}{2}$ of the SEPS electronics system.

neutral atoms) component. Over the polar cap region, near apogee, where energetic ion backgrounds may be low, the ENA image may dominate on occasion for SEPS and IPS.

The electron and ion telescopes use stacks of solid-state detectors. A 200 llm thick silicon position sensitive XY detector (see Figure 20) is the outer element in each stack. A 5 mm thick SiLi detector behind each XY detector is operated in coincidence with the XY detector, and is vetoed by penetrating background signals from the opposite direction. The XY sensor has an area of 6.25 cm^2, and is divided into 256 individually read out pixels. It was developed especially for SEPS by Hamamatsu Inc. In contrast to strip detectors, the individual pixels have smaller capacitance, exhibit less crosstalk, and allow for fast parallel processing. The proton dead layer was found to be 8 keV; the energy resolution of a single pixel at room temperature is 2 keV FWHM. Six of these sensors (using 768 amplifier strings) are implemented in SEPS. To eliminate single point failures SEPS is split into two independent halves: two power supplies, two processors, two PHA sections, and two detector sections.

4.2. DATA PROCESSING ELECTRONICS

A system diagram of one half of the instrument electronics is shown in Figure 20. The particle direction and identification are obtained from the logic conditions established between the various elements of the telescope. The very compact, low power SEPS electronics incorporate three types of semi-custom analog/digital gate arrays two of which are used as chip-on-board. Data are acquired and processed in 48 parallel channels, each handling a group of 16 pixels. Every pixel generates two 16-channel spectra accumulated in a dedicated RAM. Programmable coincidence logic selects the events which are processed. Ninety-six 17-bit scalers sample all of the pixel counting rates as well as several veto rates. An on-board, computer-controlled calibration pulser, connected to individual pixel inputs is used periodically to test and calibrate the entire system.

Three low-power (CMOS), radiation hardened gate-array microcircuits, jointly developed with KMOS, Inc., are used in the SEPS instrument. As mentioned above, two of these microcircuits are mounted directly to the rigid-flex printed wiring board using sealed chip-on-board. This configuration results in minimum stray capacitance and high packaging density.

The first of these two chips is the front-end (FE) microcircuit. Each of the FE microcircuits (54 in SEPS) has 16 low noise amplifier strings with associated coincidence logic. Individual pulses are amplified and shaped for subsequent peak holding. These data are passed to the second microcircuit for pulse height analysis.

The second gate array microcircuit is a 16 channel pulse height analyzer (PHA) microcircuit (12 are used in SEPS). Each chip processes data from four FE microcircuits by polling every 8 ms. The PHA consists of programmable 16-channel stacked discriminators (log/linear) with eight 16-bit scalers, and a 16-bit computer bus. The state logic directs the collection and storage of spectra in a separate dedicated 8 K $\times$ 8 RAM.

A versatile input/output (IO) interface between the onboard microprocessor and the instrument or spacecraft is provided by the third microcircuit (IO) developed for SEPS. Programmable control registers are used to configure the chip. Some of the features included in the microcircuit are: a 16-bit computer interface with 4-bit address decode, a serial input/output, an 8-bit counter/timer, a watch-dog timer, a digital-to-analog converter with pulser calibration, an analog-to-digital converter, and dual 8-bit bi-directional parallel ports. This chip uses $<$20 mW of power.

Two Central Processor Units (CPUs), either of which can be the master, control the instrument and act as the SEPS DPU. The 80C86 CPUs, with 96K of RAM and 16 K PROM, collect, process, and format the SEPS data. The internal data collection rate is much higher than the telemetry rate (1.18 Kbits); thus, these data must be selected, combined, and compressed. The science portion of the telemetry format and the on-board processing can be changed by command.

In order to investigate the full matrix of data inputs from the SEPS detectors over a short interval, a burst memory was required. Data can be accumulated at up to 100 samples s^{-1} for each of the XY sensors, and stored in the 16 Mbit memory. These fast, snapshot/movie data will be used mainly in special regions of interest (auroral and wave-particle regions) where the flux is varying rapidly with a high enough intensity to give meaningful statistics. These burst data will be played back through the SEPS/PIXIE interface ($\sim$ 3.0 kbits s^{-1}), and in a portion of the SEPS telemetry.

4.3. Telemetry, Control, and Data Processing Software

Data for the SEPS instrument is processed internally and sent directly to the spacecraft through the SEPS spacecraft interface or through the SEPS/PIXIE SWAP interface. The SWAP interface allows SEPS to use a large portion of the PIXIE telemetry stream during regions where the PIXIE data is less interesting due to background contamination. The SEPS sensors provide 256 electron pixel telescope elements, and 128 ion pixel telescope elements viewing up and down. These data are selected, combined, and compressed by on-board processing since the telemetry rate is much smaller than the data acquired. The science data consist of: 16 energy channels/mode from 768 XY pixels, 6 E sensors, and associated coincidence and anticoincidence scaler rates. All selected science data are logarithmically compressed to 8 bits. In addition to the fixed SEPS telemetry data set, the standard operating modes are the loss-cone mode, the matrix scan mode, and burst data mode. In the loss-cone mode, data are formatted according to a pitch angle scan with 16-channel energy resolution, pitch angle data emphasizing time resolution, or flux in the loss-cone with good energy and time resolution. In the matrix scan mode, the full pixel matrix is read out with 16-channel energy resolution. Burst mode allows high time resolution for energy, flux, and pitch angle. An onboard burst memory of 16-Mbits is used to store particle image data over selected fields of view with >1 ms image periods.

5. Discussion and Summary

Fulfilment of the scientific objectives, discussed in Section 1 above and summarized in Table I, called for the development of an experiment payload with a rather special set of properties, as outlined in Section 2. In meeting the challenges posed by the science and spacecraft requirements, it was often not only necessary to use existing state-of-the-art techniques and hardware, but to develop new ones and adapt them to space applications. Especially noteworthy in this regard are the custom analog/digital KMOS gate arrays (used in the IPS, and SEPS), the RAL charge-to-voltage converter (used in the IES), the Actel programmable gate arrays (used extensively in both DPUs). Without the use of the surface mount, chip-on-board, and rigid-flex fabrication technologies, meeting the weight, volume and

power constraints would have been impossible. The resultant investigation not only meets the stringent power, volume, and weight limits, but possesses the heretofore unachieved, rapid (6 s) imaging capability of the unit sphere, with high dynamic range in energy and countrate space, while maintaining fine energy resolution.

Acknowledgements

At Aerospace, we would like to express special thanks to Rich Gerardi, Art McClellan, and Joe Stein for their efforts to achieve compliance with the plethora of NASA rules and regulations. In this they were helped immensely by Don Crosby, Jim Lohr, and Tom Taylor of NASA, and we greatly appreciate that help. We would also like to thank Bill Skinner for his mechanical design efforts, Norm Katz, Dave Lau, Van Tran, Vince Hunt, Carl Ibscher, Don Katsuda and Mark Lalic for their help in the electronic development, and Kirk Crawford, Sam Imamoto, Joel Kirshner, Patty Lew, and Bob Walter for their assistance with development of the ground support equipment and sensor calibration. The Aerospace portion of the work was funded by NASA under Contract No. NAS5-30368.

The LANL authors wish to acknowledge the great effort of our technicians, Leroy Cope and Robert 'Chuck' Clanton, during the development and testing of the IES and HIST as well as Dr Robert Nemzek for the testing of the IES. Finally, we want to express our thanks to Bob Hedges for project management on the first phases of the project and Dr Donald Cobb for the overall management of the LANL effort. The LANL portion of the CEPPAD effort was funded by NASA under Contract No. NDPRS-19511 E.

At LPARL, would like to thank Dr J. B. Reagan for his many contributions to the initial SEPS proposal, and express our gratitude to Drs R. R. Vondrak, T. R. Fisher, L. F. Chase, and M. Walt for their programmatic contributions. We greatly appreciate the efforts at Lockheed of B. J. Costanzo, J. Gates, C. W. Gilbreth, B. Gordon, D. Lose, E. L. McFeaters, D. O. Murray, G. S. F. Orsten, M. L. Peloquin, L. A. Reed, R. R. Robinson, K. G. Strickler, and J. J. Suty. The efforts of R. B. Kash, and A. J. Goodwater of KMOS are appreciated in the development of the SEPS, and IPS mixed-mode gate array microcircuits. We also greatly appreciate the contributions of T. S. Taylor, and D. Chaffey of NASA/GSFC, and Mr P. A. Harris of MMC. Funding for the LPARL portion of the effort was provided under NASA Contract No. NAS5–30622.